DMD Fast Forward. Published on September 12, 2018 as DOI: 10.1124/dmd.118.081919
This article has not been copyedited and formatted. The final version may differ from this version.

DMD # 81919

Metabolism of c-Met kinase inhibitors containing quinoline by aldehyde oxidase, electron donating and steric hindrance effect

Jiang Wei Zhang, Wen Xiao, Zhen Ting Gao, Zheng Tian Yu, Ji Yue (Jeff) Zhang

China Novartis Institutes for Biomedical Research, 4218 Jinke Road, Shanghai 201203, China

DMD # 81919

Running title: Electron donating and steric hindrance effect on AO

Address correspondence to:

Jiang Wei Zhang

China Novartis Institutes for BioMedical Research Co., Ltd.

F2B4, Novartis Campus, No.4218 Jinke Road, Pudong, Shanghai 201203, China

Email: jiangwei.zhang@novartis.com

Ji Yue (Jeff) Zhang

China Novartis Institutes for BioMedical Research Co., Ltd.

F2B4, Novartis Campus, No.4218 Jinke Road, Pudong, Shanghai 201203, China

Email: jeff.zhang@novartis.com

Number of Text Pages: 33

Number of Tables: 5

Number of Figures: 5

Number of References: 32

Number of Words

In the Abstract: 211

In the Introduction: 375

In Discussion: 1150

Abbreviations:

AO, aldehyde oxidase; XO, xanthine oxidase; MRM, multiple reaction monitoring; ΔG, energy needed to form tetrahedral intermediate from substrate and H_2O; EDG, electron donating group; c-Met, Mesenchymal-epithelial transition factor

Abstract

Some quinoline containing c-Met kinase inhibitors are aldehyde oxidase (AO) substrates. 3-substituted quinoline triazolopyridine analogues were synthesized to understand the electron donating and steric hindrance effect on AO-mediated metabolism. Metabolic stability studies for these quinoline analogues were carried out in liver cytosol from mice, rats, cyno monkeys, and humans. Several 3-N-substituted analogues were found to be unstable in monkey liver cytosolic incubations ($t_{1/2}$ < 10 min), and five of them (**63**, **53**, **51**, **11,** and **71**) were chosen for additional mechanistic studies. Monooxygenation on the quinoline ring was identified by LC/MS/MS. Metabolite formation was inhibited by the AO inhibitors menadione and raloxifene, but not by the xanthine oxidase inhibitor allopurinol. It was found that small electron donating groups at the 3-quinoline moiety made the analogues more susceptible to AO metabolism, while large 3-substituents could reverse the trend. Although species differences were observed, this trend was applicable to all species tested. Small electron donating substituents at the 3-quinoline moiety increased both affinity (decreased K_m) and V_{max} towards AO in kinetic studies, while large substituents decreased both parameters probably due to steric hindrance. Based on our analysis, a common structural feature with high AO liability was proposed. Our finding could provide useful information for chemists to minimize potential AO liability when designing quinoline analogues.

DMD Fast Forward. Published on September 12, 2018 as DOI: 10.1124/dmd.118.081919
This article has not been copyedited and formatted. The final version may differ from this version.

Introduction

c-Met is a receptor tyrosine kinase for hepatocyte growth factor. c-Met over-expression and mutation are associated with tumorigenesis, metastasis, poor prognosis, and drug resistance (Cañadas *et al.*, 2010; Liu *et al.*, 2010; Parikh and Ghate, 2018). c-Met has become an attractive target for non-small cell lung cancer and other advanced cancer, resulting in many small-molecule c-Met inhibitors in clinical trials (Fig. 1)(Cañadas *et al.*, 2010; Liu *et al.*, 2010; Cui *et al.*, 2013; Cui, 2014).

Aldehyde oxidase (AO) plays an important role in the metabolism of aromatic aza-heterocycles (Kitamura *et al.*, 2006; Pryde *et al.*, 2010). As an aza-heterocycle, quinoline is an essential binding motif in class Ib selective c-Met inhibitors, such as capmatinib, OMO-1, AMG-208, SGX523, JNJ-38877605, and PF-04217903 (Fig. 1) (Cui, 2014). Many quinoline containing c-Met kinase inhibitors were reported to be AO substrates including SGX523 and JNJ-38877605 (Diamond *et al.*, 2010; Lolkema *et al.*, 2015). The C-H bond at the 2-quinoline position was metabolized by human AO to form a lactam metabolite (Kitamura *et al.*, 2006; Pryde *et al.*, 2010). Being less soluble and prone to crystallize in the kidney, the lactam metabolite was believed to be the culprit of nephrotoxicity and ultimately clinical failure for SGX523 and JNJ-38877605 (Diamond *et al.*, 2010; Lolkema *et al.*, 2015). To overcome AO metabolism related low solubility issue, some efforts have been made to modify the quinoline moiety, such as converting it to an imidazopyridine moiety in volitinib (Jia *et al.*, 2014), or replacing it with an isoquinolinone moiety (Ryu *et al.*, 2011). In addition, no AO liability was observed when some bulky substituents were added at the 3-quinoline (Zhao *et al.*, 2017). We have discovered a series of triazolopyridine analogues as potent c-Met inhibitors, and have attempted to add N-substituents at the 3-quinoline to block or reduce AO-mediated metabolism (Chen

et al., 2013). However, several of these substituted analogues were found unstable in cytosolic stability assay, suggesting they were still liable for AO-mediated metabolism.

This study was aimed to evaluate the relationship between AO metabolism and quinoline with different N-substituents at the 3-position for triazolopyridine c-Met inhibitors. Electron donating groups (EDG) and steric hindrance were found to affect AO metabolism. Our findings could provide useful information for chemists to minimize potential AO liability when designing quinoline analogues.

Materials and methods

Chemicals

Triazolopyridine compounds, SGX523, and INC280 were synthesized at China Novartis Institute of Biomedical Research (Shanghai, China) (Chen *et al.*, 2013). Allopurinol and menadione were purchased from Sigma-Aldrich (St. Louis, MO, USA). Raloxifene was purchased from Shanghai DEMO Medical Tech Co. Ltd. Pooled mouse liver cytosol (male CD1, n=1000) and pooled rat liver cytosol (male IGS SD, n=400) were purchased from Xenotech (Lenexa, KS, USA). Pooled monkey liver cytosol (male cyno) was purchased from IPhase Pharma Service (Beijing, China). Pooled human liver cytosol (Ultrapool 150) was purchased from BD Biosciences (San Jose, CA, USA). All other reagents were of HPLC grade or of analytical grade.

Metabolic stability

Parent compound depletion in cytosolic incubation was used to measure metabolic stability. The incubation, with a total volume of 200 μL, was conducted in 50 mM potassium phosphate buffer (pH 7.4) with liver cytosol (2 mg/ml), and test compounds (1 μM). Test compounds were dissolved in DMSO to 10 mM, then further diluted in water to 2 μM. The final concentration of DMSO was < 0.1% for all incubations. After 15-min pre-incubation at 37°C, the reaction was initiated by adding the test compound. After 0, 30, 60, and 120 min incubation at 37°C, 40-μL aliquots were removed and mixed with 100 μL ACN containing internal standard (I.S.) to terminate the reaction. The mixture was centrifuged at 3,400× *g* for 10 min at room temperature. The supernatants (50 μL) were diluted with Milli-Q water (50 μL) and analyzed by LC/MS. The mass response of the parent compound at 0 min was set at 100%. The rate constant of substrate depletion, *k*,

DMD Fast Forward. Published on September 12, 2018 as DOI: 10.1124/dmd.118.081919
This article has not been copyedited and formatted. The final version may differ from this version.

was the slope of the semi-logarithmic plot of the percentage remaining versus time. In vitro half-life ($t_{1/2}$) was calculated using the equation: $t_{1/2}=\ln 2/k$.

The LC/MS/MS system consisted of Shimadzu UFLC LC20A system, AB Sciex API5000 mass spectrometer, and Chromolith@FastGradient C18 column (2.0 x 50 mm, Merck, Darmstadt, Germany). The mobile phase A and B were H_2O and ACN, respectively, with 0.1% formic acid as additive in both solvents. The mobile phase B was increased from 2% to 80% over 0.3 min, and kept at 80% for another 0.4 min before being changed back to 2%. The flow rate was 600 µL/min with a total run time of 2 min. The ionization was optimized using APCI (+) and the detection was performed via multiple reaction monitoring (MRM). Other mass parameters were: collision gas at 6 psi, curtain gas at 35 psi, ion source gas 1 at 50psi, temperature at 450°C, nebulizer current at 3 V, entrance potential at 10 V, and collision cell exit potential at 15 V.

Metabolite identification

The incubation system was similar to that mentioned above in the metabolic stability study. Briefly, in a total volume of 200-µL incubation system, the test compound (5 µM) was incubated with 1.0 mg/ml monkey liver cytosol in potassium phosphate buffer (pH 7.4, 50 mM) at 37°C for 120 min. The reaction was terminated by adding 400-µL ACN. After centrifugation, the supernatant was then transferred into a new vial and evaporated to dryness in vacuo. The residue was reconstituted with 100 µL of 50% ACN in H_2O and subjected to direct LC/MS/MS analysis. The LC/MS/MS system was a Thermo Accela HPLC coupled with a Thermo LTQ OrbriTrap XL ion-trap mass spectrometer (Thermo-Fisher Scientific, Waltham MA, USA) and an Agilent XDB-C_{18} column (4.6 x 50 mm, 1.8 µm, Santa Clara, CA, USA). The mobile phase A was 0.1% formic acid in water and mobile phase B was 0.1% formic acid in acetonitrile. The mobile phase B was increased

DMD Fast Forward. Published on September 12, 2018 as DOI: 10.1124/dmd.118.081919
This article has not been copyedited and formatted. The final version may differ from this version.

from 2% B to 98% B over 20 min using a flow rate of 300 μL/min. The mass spectrometer was operated in a positive ion mode with an electrospray ionization source. Samples were analyzed using a linear ion trap Q1 scan with Information Dependent Acquisition (IDA) triggered product ion (MS2) scans. Detailed instrument settings were listed as follows: capillary temperature at 275 °C; sheath gas flow at 10 psi; source voltage at 4.5 kV; capillary voltage at 24 V.

Chemical inhibition

Compounds **63**, **53**, **51**, **11**, and **71** were selected for chemical inhibition study in human liver cytosol because of their high metabolism conversion rates. Chemical inhibition studies were performed by adding various molybdenum hydroxylase inhibitors to identify the enzyme responsible for the metabolism. In a total 50-μL incubation system, each compound (5 μM) was incubated with human liver cytosol (0.5 mg/ml) for 30 min. Various molybdenum hydroxylase inhibitors and their final concentrations were listed as follows: menadione (50 μM) (Johns, 1967), raloxifene (20 μM) (Obach, 2004), and allopurinol (50 μM) (Massey *et al.*, 1970). These chemical inhibitors were dissolved in DMSO and diluted with water to produce working solutions. For all the experiments, the final concentration of DMSO was less than 0.15% (v/v). In the controls, equal volume of solvent was added. There was 10 min pre incubation, and the reaction was initiated by the addition of the substrate. The termination, centrifugation, and dilution steps were the same as in the metabolic stability study. A 5-μM concentration was selected around the K_m value so that detectable metabolite could be produced. Oxidative metabolites were detected by LC/MS using predictive MRM methods deriving from their corresponding parent compounds. The predicted MRMs for oxidative metabolites (M) and their parent compounds (P) were listed as follows: **63** (P: 359 → 173, M: 375 → 173); **53** (P: 418 → 146, M: 434 → 146); **51** (P: 444 → 146, M: 460 → 146); **11** (P: 458 → 173, M: 474 →

DMD Fast Forward. Published on September 12, 2018 as DOI: 10.1124/dmd.118.081919
This article has not been copyedited and formatted. The final version may differ from this version.

173); and **71** (P: 430 → 400, M: 446 → 416). All incubations were performed in duplicate unless stated otherwise.

Kinetic studies

To estimate kinetic parameters, test compounds were incubated with liver cytosol from different species for 30 min. The incubation conditions such as substrate and cytosol concentrations were listed in Table 1. The apparent V_{max} and K_m values were calculated by nonlinear regression analysis of experimental data according to the Michaelis-Menten equation. Preliminary experiments were performed to make sure that formations of metabolites were in the linear range for both reaction time and cytosol concentration. The metabolites were measured using a MRM mode. Due to the lack of metabolite standards, the quantifications were based on the calibration curves from corresponding parent compounds (5-1000 nM), assuming similar mass response. All incubations were performed in duplicate with SD values generally below 10%.

In silico methods

During AO catalyzed oxidation process, the formation of a tetrahedral intermediate (-CHOH-NH-) was hypothesized by adding H_2O to the substrate on the -C=N- double bond (Torres *et al.*, 2007; Dalvie *et al.*, 2012; Xu *et al.*, 2017). The energy required to form the tetrahedral intermediate (ΔG) is defined as follows: $\Delta G = G_{inter}-G_{sub}-G_{H2O}$, where G_{inter}, G_{sub}, and G_{H2O} represent the single point energy of intermediate, substrate, and water, respectively. Single point energy was calculated according to the methods reported (Torres *et al.*, 2007; Dalvie *et al.*, 2012; Xu *et al.*, 2017) with slight modifications. Briefly, 3D structures were firstly optimized by Spartan 06 (Wavefunction Irvine, CA, USA) using the minimization function. Then single point energy was determined by

Spartan using the B3LYP/6-31G** basis set. No solvent model was considered during the calculation.

Docking studies

To evaluate steric hindrance effect, molecular volume was calculated and ligands were docked into the active site of AO receptor (PDB entry 4uhx) (Coelho et al., 2015). Focus 3.83 software (Molsoft L.L.C., San Diego CA) was used for molecular volume calculation and docking studies (Stiefl *et al.*, 2015). Both the ligands and the receptor were optimized in Focus before docking. A 40 × 40 × 40 point grid centered on phthalazine was used a docking region. The productive pose with the lowest docking score was used for analysis.

Results

Metabolic stability

Metabolic stability of quinoline analogues was carried out in liver cytosol isolated from mice, rats, cyno monkeys, and humans (Table 2). SGX523 and INC280 were included as controls, and the $t_{1/2}$ values were listed in supplemental Table 1. **63** had no substituent on the quinoline moiety, and showed slow turnover in liver cytosolic incubation with $t_{1/2}$ > 500 min in all four species tested. Some small N-substituents at the 3-position made the compounds unstable. Half-lives less than 10 min were observed for **53**, **51**, and **71** in monkey liver cytosolic incubations (Table 2). Similarly, these compounds were also unstable in liver cytosolic incubation from mice, rats, and humans. Based on the $t_{1/2}$ values, AO activity was the highest in monkeys, followed by mice, and the lowest in rats and humans for **68, 53, 51,** and **71**. This rank of order was not applicable to **11**, **47**, and **15**. Therefore, species difference seemed to be compound specific and there was no constant pattern (Sahi *et al.*, 2008).

As the size of N-substituent increased, the compounds became more stable (longer $t_{1/2}$). $T_{1/2}$ > 2h was observed in all four species for **68**, **2**, **23**, **5**, **15**, **47**, and **12**. Compared with **51**, **11** had only one extra methylene linker and its $t_{1/2}$ value was much longer (144 min versus 3 min in the monkey). The lowest molecule volumes were observed for **53**, **51**, and **71**, corresponding to the least stable compounds in the list (Table 2). These observations showed that small EDG substituents increased AO-mediated metabolism, while large substituents had an opposite effect probably due to steric hindrance.

Metabolites identification

The least stable compounds (**53**, **51**, **11**, and **71)** were chosen for metabolite identification study in monkey liver cytosol. **63** was included for the comparison. Monooxygenated metabolites (m/z +16) with longer LC retention time than parent

compounds were observed for these compounds in LC/MS (Fig. 2). The yields were 83% (**71**), 75% (**51**), 57% (**53**), 13% (**11**), and 3% (**63**) after 2-h incubation. Compared with **63**, N-substituents at the 3-position of quinoline moiety made compounds less stable in cyno monkey liver cytosol, as the yield increased. A large N-substituent at the 3-position (**11**) reduced the yield, indicating steric hindrance effect. This finding is consistent with the results obtained in metabolic stability study.

The MS/MS fragments of parent compounds and their proposed metabolites were listed in Table 3 and supplemental Figure 1. The oxidation was proposed to occur on the quinoline part of the molecule based on MS/MS fragmentation. Many studies showed the vacant C-H adjacent to the nitrogen atom in an aromatic heterocycle was metabolized to form a lactam metabolite by molybdenum hydroxylase (Kitamura *et al.*, 2006; Pryde *et al.*, 2010). The 2-quinoline was assumed to be oxidized to yield a lactam accordingly (Table 3). The structure assignment was consistent with a longer retention time of 2-oxo-quinoline metabolite compared with the parent compound observed for quinoline containing c-Met inhibitors such as SGX523, capmatinib, and many others (Diamond *et al.*, 2010; Xu *et al.*, 2017; Dick, 2018). No further study was made to confirm the metabolite structures.

Chemical inhibition

Molybdenum hydroxylase was involved in the oxidative metabolism of these quinoline analogues in cytosol without NADPH. To identify the enzyme involved in the metabolism, molybdenum hydroxylase inhibitors were added to the incubation system. Allopurinol (XO inhibitor) exhibited limited or no inhibition (<17%) towards all the analogues tested. Both menadione and raloxifene (AO inhibitors) inhibited over 75% of metabolite formation of **63**, **53**, **51**, and **71** (Table 4, Fig. 3). For **11**, the metabolite formation was inhibited by 51% (menadione) and 35% (raloxifene) in human liver cytosolic incubation.

DMD Fast Forward. Published on September 12, 2018 as DOI: 10.1124/dmd.118.081919
This article has not been copyedited and formatted. The final version may differ from this version.

Relatively low inhibition of **11** in human liver cytosolic incubation was probably due to its low conversion rate. Therefore, inhibition study was repeated in mouse liver cytosol, in which a high conversion rate was observed for **11**. The metabolism of **11** was inhibited 93% and 86% by menadione and raloxifene, respectively. This data revealed that AO and not XO was the enzyme responsible for the quinoline metabolism.

Kinetic study

To further explain the observed differences in the metabolism of quinoline analogues, kinetic studies were performed in four species (Fig. 4, Table 5). In agreement with the metabolite identification study, **63** had the lowest clearance judging from V_{max}/K_m value (< 0.5 µL/min/mg). The N-substituent at the 3- position of the quinoline moiety increased AO metabolism (increased V_{max}/K_m value). Compared with **63**, decreased K_m values were observed for all N-substituent analogues in all species, indicating increased binding affinity. Compared with **63**, increased V_{max} values were observed for all compounds in all species except for **11** and **51** in human liver cytosol (Fig. 4, Table 5). **11** had the lowest V_{max}/K_m value among N-substituent analogues, again suggesting that large N-substituents impede AO metabolism by steric hindrance. Species differences were also observed. Cyno monkeys had the largest V_{max} value for **71**, **11**, and **51**; while V_{max}/K_m value was the highest in mice for **11**, **51**, **53**, and **63**. The lowest V_{max}/K_m value was observed in humans for **71**, **11**, and **51**.

DMD Fast Forward. Published on September 12, 2018 as DOI: 10.1124/dmd.118.081919
This article has not been copyedited and formatted. The final version may differ from this version.

Discussion

There are many c-Met inhibitors containing a quinoline moiety in the clinical trials (Fig. 1) (Cui, 2014), and AO has been reported to play a major role in the quinoline metabolism (Xu *et al.*, 2017). Clinical failure of SGX523 and PF-4217903 was reported due to the low solubility of their AO-mediated metabolites, which precipitated in the kidney and led to renal failure (Diamond *et al.*, 2010; Lolkema *et al.*, 2015). A novel series of 3-N-substituted quinoline triazolopyridine analogues were discovered as potent c-Met inhibitors with a clean PDE3 profile (Chen *et al.*, 2013). To monitor AO-mediated metabolism, AO liability was routinely screened in monkey liver cytosol. In theory, extra substituents should increase steric hindrance to deter AO metabolism. However, several 3-substituted quinoline analogues were found less stable than the unsubstituted quinoline. This prompted us to investigate the mechanism.

In the present study, cytosol was used to measure AO metabolism. Selection of cytosol would exclude other metabolizing enzymes or transporters and simplify the system to consider cytosolic enzymes only. The site of metabolism was ascribed to the quinoline moiety based on the MS/MS fragmentation and the characteristic longer retention time as compared with the parent compound. Additional chemical inhibition study revealed AO but not XO was the principal metabolizing enzyme. Small electron donating N-substituents on the 3-quinoline increased AO metabolism, while bulky N-substituents would exhibit steric hindrance effect. The EDG and steric hindrance effect observed in this study were in agreement with these reported (Jones and Korzekwa, 2013; Lepri *et al.*, 2017; Xu *et al.*, 2017).

Molybdenum hydroxylases catalyzed oxidation by nucleophilic attack at the carbon atom adjacent to the nitrogen in aromatic heterocycles (Pryde *et al.*, 2010). The energy needed to form the tetrahedral intermediate (ΔG) was used to predict AO metabolism

DMD Fast Forward. Published on September 12, 2018 as DOI: 10.1124/dmd.118.081919
This article has not been copyedited and formatted. The final version may differ from this version.

(Torres *et al.*, 2007). And low ΔG value favors AO metabolism (shorter half-life). ΔG values were calculated and the results were shown in Table 2. Lower ΔG values were observed for all 3-N-substituted quinoline compounds. ΔG values of at least 4 kcal/mol lower than **63** were observed for the high clearance compounds **53, 51**, **11** and **71**. However, low ΔG values were also observed for **68**, **23**, **5**, and **15** (< 10.7 kcal/mol), rather stable compounds. These observations suggest ΔG value alone cannot predict AO stability.

Besides ΔG, steric hindrance was reported as another main factor affecting AO metabolism (Torres *et al.*, 2007; Dalvie *et al.*, 2012; Lepri *et al.*, 2017; Xu *et al.*, 2017). To evaluate the steric hindrance effect, these analogues were docked to the active site of AO (PDB entry 4uhx) (Coelho *et al.*, 2015), and docking scores were listed in Table 2. Docking score can reflect the steric hindrance effect among ligand binding, and a lower docking score favors the reaction. Docking score of more than 2 units lower was observed for good AO substrates such as **53, 51**, and **71**. Low docking scores were probably due to the extra hydrogen bond formation. The tetrahydrofuran or oxetane moiety in **51** and **71** provided a hydrogen bond acceptor for residue **G1019**, and the hydroxyl group in **53** supplied both a hydrogen bond acceptor and a donor for residue **G1017** and **G1088**, respectively. Higher docking scores were observed for other analogues. The $t_{1/2}$ difference between two matched pairs (**51** versus **5**, and **68** versus **23**) probably implied the hydrogen bond donor was not well tolerated. Primary and secondary amines analogues (**2**, **23**, and **5)** were stable in cytosol (Table 2).

Many 4- or 5- linked quinoline compounds were AO substrates with high clearance and short $t_{1/2}$ in cytosol, such as ML-347, LDN-193189, A-77-01, zoniporide, and SB-277011 (Austin *et al.*, 2001; Dalvie *et al.*, 2012; Dick, 2018). However, 6-linked quinoline c-Met inhibitors such as SGX523 (Diamond *et al.*, 2010), PF-4217903 (Zientek *et al.*, 2010; Xu

et al., 2017), BVU972 (Xu *et al.*, 2017), and INC280 (Xu *et al.*, 2017; Dick, 2018) were more stable. **63** is an AO substrate, but like those 6-linked quinoline c-Met inhibitors, its AO metabolism rate was slow ($t_{1/2}$ > 2h) in cytosolic incubations from both rodents and primates (Table 2). These data could explain why so many 6-linked quinoline c-Met inhibitors are in the clinical despite AO-mediated metabolism. ΔG (kcal/mol) for these 4- or 5- linked quinoline compounds was calculated to be 13.4 (ML-347), 15.8 (LDN-193189), 20.5 (A-77-01), 10.6 (zoniporide), and 19.3 (SB-277011). The low ΔG could explain the short $t_{1/2}$ for zoniporide. For ML-347, LDN-193189, A-77-01, and SB-277011, their ΔG values were comparable or even higher than **63**. Therefore their high AO-mediated metabolism rates were not caused by electron effect such as ΔG. These observations may suggest the quinoline linkage positions exert different steric hindrance effect and the 6-linkage is generally more resistant to AO metabolism than the 4-, or 5-linkage.

AO-mediated metabolism can also occur to the heterocyclic core moiety besides the quinoline for some c-Met inhibitors. For example, AO metabolite formed on the heterocyclic core moiety instead of the quinoline was the major metabolite for capmatinib (Xu *et al.*, 2017; Dick, 2018). Similarly, AO oxidation exclusively on the imidazole core moiety was observed for c-Met inhibitor **compound 1** (Zhao *et al.*, 2017). Many of our own c-Met inhibitors with $t_{1/2}$ <3 min in cytosolic incubations were also mainly metabolized by AO on the heterocyclic core moiety instead of the 6-linked quinolines (Unpublished data, Fig. 5). Like **71**, EDGs such as O- and NH-linked cyclopropylmethyl moiety (**Unpublished example 1** and **2**, Fig. 5) were observed for these compounds unstable in cytosol. Besides aromatic aza-heterocycle with a vacant C-H adjacent to a nitrogen atom (Pryde *et al.*, 2010), it seems EDG (N, O, phenyl) nearby would make the heterocycle core ring more vulnerable to AO metabolism. Several AO substrates with

similar substructure from literature were listed in Fig. 5. A *meta*-O-linked EDG in XK-469 (Anderson *et al.*, 2005; Hutzler *et al.*, 2012) and VU0409106 (Morrison *et al.*, 2012), or *meta*-N-linked EDG in **example 2**, **20** (Lepri *et al.*, 2017; Cruciani *et al.*, 2018) and **30** (Glatthar *et al.*, 2016) made these compounds more susceptible to AO metabolism (Fig. 5). Based on the examples from literature and those we encountered in our internal c-Met program, a structural feature with potentially high AO liability was proposed as follows: 1) aza-heterocycle, 2) *o*-vacant C-H, 3) *m*-small electron donating group (N, O, phenyl, etc.) (Fig. 5). It should be noted this substructure is not automatically translated to AO substrate, since steric hindrance also plays a major role, as observed in this study.

In summary, EDG and steric hindrance affect AO-mediated metabolism. For the triazolopyridine series of c-Met inhibitors, an unsubstituted quinoline is a poor AO substrate, and small substituents of EDG at the 3-quinoline increase AO metabolism rate by decreasing the ΔG, while large substituents impede AO metabolism due to steric hindrance.

Acknowledgments

The contributions of Novartis c-Met project team members, especially GDC Shanghai colleagues are greatly acknowledged. We'd like to thank Jane W. Zhang from Yale University for proofreading the manuscript.

Authorship Contributions

Participated in research design: Jiang Wei Zhang, Ji Yue (Jeff) Zhang

Conducted experiments: Jiang Wei Zhang, Wen Xiao, Zhen Ting Gao

Contributed new reagents or analytic tools: Jiang Wei Zhang, Wen Xiao, Zhen Ting Gao, Zheng Tian Yu

Performed data analysis: Jiang Wei Zhang, Wen Xiao, Zhen Ting Gao, Zheng Tian Yu, Ji Yue (Jeff) Zhang.

Wrote or contributed to the writing of the manuscript: Jiang Wei Zhang, Ji Yue (Jeff) Zhang

Reference

Anderson LW, Collins JM, Klecker RW, Katki AG, Parchment RE, Boinpally RR, LoRusso PM, and Ivy SP (2005) Metabolic profile of XK469 (2(R)-[4-(7-chloro-2-quinoxalinyl)oxyphenoxy]-propionic acid; NSC698215) in patients and in vitro: low potential for active or toxic metabolites or for drug-drug interactions. *Cancer Chemother Pharmacol* **56**:351–7.

Austin NE, Baldwin SJ, Cutler L, Deeks N, Kelly PJ, Nash M, Shardlow CE, Stemp G, Thewlis K, Ayrton A, and Jeffrey P (2001) Pharmacokinetics of the novel, high-affinity and selective dopamine D3 receptor antagonist SB-277011 in rat, dog and monkey: in vitro/in vivo correlation and the role of aldehyde oxidase. *Xenobiotica* **31**:677–686.

Cañadas I, Rojo F, Arumí-Uría M, Rovira A, Albanell J, and Arriola E (2010) C-MET as a new therapeutic target for the development of novel anticancer drugs. *Clin Transl Oncol* **12**:253–60.

Chen C, Deng H, Guo H, He F, Jiang L, Liang F, Mi Y, Wan H, Xu Y-C, Yu H, and Zhang JY (Jeff) (2013) 6 - substituted 3 - (quinolin- 6 - ylthio) - [1,2,4] triazolo [4, 3 -a] pyradines as tyrosine kinase. WO/2013/038362, PCT, China.

Coelho C, Foti A, Hartmann T, Santos-Silva T, Leimkühler S, and Romão MJ (2015) Structural insights into xenobiotic and inhibitor binding to human aldehyde oxidase. *Nat Chem Biol* **11**:779–783.

Cruciani G, Milani N, Benedetti P, Lepri S, Cesarini L, Baroni M, Spyrakis F, Tortorella S, Mosconi E, and Goracci L (2018) From Experiments to a Fast Easy-to-Use Computational Methodology to Predict Human Aldehyde Oxidase Selectivity and Metabolic Reactions. *J Med Chem* **61**:360–371.

Cui JJ (2014) Targeting receptor tyrosine kinase MET in cancer: small molecule inhibitors and clinical progress. *J Med Chem* **57**:4427–53.

Cui JJ, Shen H, Tran-Dubé M, Nambu M, McTigue M, Grodsky N, Ryan K, Yamazaki S, Aguirre S, Parker M, Li Q, Zou H, and Christensen J (2013) Lessons from (S)-6-(1-(6-(1-methyl-1H-pyrazol-4-yl)-[1,2,4]triazolo[4,3-b]pyridazin-3-yl)ethyl)quinoline (PF-04254644), an inhibitor of receptor tyrosine kinase c-Met with high protein kinase selectivity but broad phosphodiesterase family inhibition leadi. *J Med Chem* **56**:6651–65.

Dalvie D, Sun H, Xiang C, Hu Q, Jiang Y, and Kang P (2012) Effect of structural variation on aldehyde oxidase-catalyzed oxidation of zoniporide. *Drug Metab Dispos* **40**:1575–1587.

Diamond S, Boer J, Maduskuie TP, Falahatpisheh N, Li Y, and Yeleswaram S (2010) Species-specific metabolism of SGX523 by aldehyde oxidase and the toxicological implications. *Drug Metab Dispos* **38**:1277–85.

Dick RA (2018) Refinement of In Vitro Methods for Identification of Aldehyde Oxidase Substrates Reveals Metabolites of Kinase Inhibitors. *Drug Metab Dispos* **46**:846–859.

Glatthar R, Stojanovic A, Troxler T, Mattes H, Möbitz H, Beerli R, Blanz J, Gassmann E, Drückes P, Fendrich G, Gutmann S, Martiny-Baron G, Spence F, Hornfeld J, Peel JE, and Sparrer H (2016) Discovery of imidazoquinolines as a novel class of potent, selective, and in vivo efficacious Cancer Osaka thyroid (COT) kinase inhibitors. *J Med Chem* **59**:7544–7560.

Hutzler JM, Yang Y-S, Albaugh D, Fullenwider CL, Schmenk J, and Fisher MB (2012) Characterization of aldehyde oxidase enzyme activity in cryopreserved human

hepatocytes. *Drug Metab Dispos* **40**:267–75.

Jia H, Dai G, Weng J, Zhang Z, Wang Q, Zhou F, Jiao L, Cui Y, Ren Y, Fan S, Zhou J, Qing W, Gu Y, Wang J, Sai Y, and Su W (2014) Discovery of (S)-1-(1-(Imidazo[1,2-a]pyridin-6-yl)ethyl)-6-(1-methyl-1H-pyrazol-4-yl)-1H-[1,2,3]triazolo[4,5-b]pyrazine (volitinib) as a highly potent and selective mesenchymal-epithelial transition factor (c-Met) inhibitor in clinical development for tre. *J Med Chem* **57**:7577–89.

Johns DG (1967) Human liver aldehyde oxidase: differential inhibition of oxidation of charged and uncharged substrates. *J Clin Invest* **46**:1492–1505.

Jones JP, and Korzekwa KR (2013) Predicting intrinsic clearance for drugs and drug candidates metabolized by aldehyde oxidase. *Mol Pharm* **10**:1262–8.

Kitamura S, Sugihara K, and Ohta S (2006) Drug-metabolizing ability of molybdenum hydroxylases. *Drug Metab Pharmacokinet* **21**:83–98.

Lepri S, Ceccarelli M, Milani N, Tortorella S, Cucco A, Valeri A, Goracci L, Brink A, and Cruciani G (2017) Structure–metabolism relationships in *human*- AOX: Chemical insights from a large database of aza-aromatic and amide compounds. *Proc Natl Acad Sci* **114**:E3178–E3187.

Liu X, Newton RC, and Scherle PA (2010) Developing c-MET pathway inhibitors for cancer therapy: progress and challenges. *Trends Mol Med* **16**:37–45.

Lolkema MP, Bohets HH, Arkenau H-T, Lampo A, Barale E, de Jonge MJ a., van Doorn L, Hellemans P, de Bono JS, and Eskens F a. LM (2015) The c-Met Tyrosine Kinase Inhibitor JNJ-38877605 Causes Renal Toxicity through Species-Specific Insoluble Metabolite Formation. *Clin Cancer Res* **21**:2297–2304.

Massey V, Komai H, Palmer G, and Elion GB (1970) On the mechanism of inactivation of xanthine oxidase by allopurinol and other pyrazolo[3,4-d]pyrimidines. *J Biol*

Chem **245**:2837–2844.

Morrison RD, Blobaum AL, Byers FW, Santomango TS, Bridges TM, Stec D, Brewer KA, Sanchez-Ponce R, Corlew MM, Rush R, Felts AS, Manka J, Bates BS, Venable DF, Rodriguez AL, Jones CK, Niswender CM, Conn PJ, Lindsley CW, Emmitte KA, and Daniels JS (2012) The role of aldehyde oxidase and xanthine oxidase in the biotransformation of a novel negative allosteric modulator of metabotropic glutamate receptor subtype 5. *Drug Metab Dispos* **40**:1834–1845.

Obach RS (2004) Potent inhibition of human liver aldehyde oxidase by raloxifene. *Drug Metab Dispos* **32**:89–97.

Parikh PK, and Ghate MD (2018) Recent advances in the discovery of small molecule c-Met Kinase inhibitors. *Eur J Med Chem* **143**:1103–1138.

Pryde DC, Dalvie D, Hu Q, Jones P, Obach RS, and Tran TD (2010) Aldehyde oxidase: An enzyme of emerging importance in drug discovery. *J Med Chem* **53**:8441–8460.

Ryu JW, Han S-Y, Yun JI, Choi S-U, Jung H, Ha J Du, Cho SY, Lee CO, Kang NS, Koh JS, Kim HR, and Lee J (2011) Design and synthesis of triazolopyridazines substituted with methylisoquinolinone as selective c-Met kinase inhibitors. *Bioorg Med Chem Lett* **21**:7185–8.

Sahi J, Khan KK, and Black CB (2008) Aldehyde oxidase activity and inhibition in hepatocytes and cytosolic fractions from mouse, rat, monkey and human. *Drug Metab Lett* **2**:176–83.

Stiefl N, Gedeck P, Chin D, Hunt P, Lindvall M, Spiegel K, Springer C, Biller S, Buenemann C, Kanazawa T, Kato M, Lewis R, Martin E, Polyakov V, Tommasi R, van Drie J, Vash B, Whitehead L, Xu Y, Abagyan R, Raush E, and Totrov M (2015) FOCUS--Development of a Global Communication and Modeling Platform for

Applied and Computational Medicinal Chemists. *J Chem Inf Model* **55**:896–908.

Torres RA, Korzekwa KR, McMasters DR, Fandozzi CM, and Jones JP (2007) Use of density functional calculations to predict the regioselectivity of drugs and molecules metabolized by aldehyde oxidase. *J Med Chem* **50**:4642–7.

Xu Y, Li L, Wang Y, Xing J, Zhou L, Zhong D, Luo X, Jiang H, Chen K, Zheng M, Deng P, and Chen X (2017) Aldehyde Oxidase Mediated Metabolism in Drug-like Molecules: A Combined Computational and Experimental Study. *J Med Chem* **60**:2973–2982.

Zhao F, Zhang LD, Hao Y, Chen N, Bai R, Wang YJ, Zhang CC, Li GS, Hao LJ, Shi C, Zhang J, Mao Y, Fan Y, Xia GX, Yu JX, and Liu YJ (2017) Identification of 3-substituted-6-(1-(1H-[1,2,3]triazolo[4,5-b]pyrazin-1-yl)ethyl)quinoline derivatives as highly potent and selective mesenchymal-epithelial transition factor (c-Met) inhibitors via metabolite profiling-based structural optimization. *Eur J Med Chem* **134**:147–158.

Zientek M, Jiang Y, Youdim K, and Obach RS (2010) In vitro-in vivo correlation for intrinsic clearance for drugs metabolized by human aldehyde oxidase. *Drug Metab Dispos* **38**:1322–7.

Figure legends

Fig. 1. c-Met inhibitors in clinical trials with quinoline or quinoline mimics. Asterisks indicate AO metabolism site.

Fig. 2. Ion extraction chromatography for selected triazolopyridine analogues and their corresponding monooxygenated metabolites. Yield is defined as the substrate conversion after test compound (5 μM) was incubated with monkey liver cytosol (1 mg/ml) for 2 hours.

Fig.3. Representative LC/MS chromatography of chemical inhibition study. AO metabolite of compound **53** appears at 1.12 min. Inhibitors used are as follows: A) solvent control; B) menadione (50 μM); C) raloxifene (20 μM); and D) allopurinol (50 μM).

Fig. 4. Michaelis-Menten plot of quinoline analogues metabolism in liver cytosol fractions from different species. Each triazolopyridine analogue (0.23-60 μM) was incubated with liver cytosol fractions (0.1-1 mg/ml) for 30 min.

Fig. 5. Proposed common structural feature with high AO liability based on AO substrates from our internal c-Met program and literature. Asterisks indicate AO metabolism site.

DMD Fast Forward. Published on September 12, 2018 as DOI: 10.1124/dmd.118.081919
This article has not been copyedited and formatted. The final version may differ from this version.

Tables

Table 1. Kinetic study conditions for triazolopyridine compounds in liver cytosol incubation from different species.

Test compound		71	11	51	53	63
Compound con.(μM)		0.23-30	0.47-60	0.23-30	0.23-30	0.47-60
Liver cytosol protein con. (mg/ml)	Monkey	0.1	0.2	0.1	0.1	1.0
	Mouse	0.5	0.5	0.5	0.5	1.0
	Human	0.5	0.5	0.5	0.5	1.0
	Rat	0.5	0.5	0.5	0.5	1.0

DMD Fast Forward. Published on September 12, 2018 as DOI: 10.1124/dmd.118.081919
This article has not been copyedited and formatted. The final version may differ from this version.

Table 2. Structure, $t_{1/2}$, molecular volume, ΔG, and docking score for the 3-substituted quinoline analogues.

$T_{1/2}$ values were determined with substrate concentration of 1 μM and liver cytosol protein concentration of 2 mg/ml.

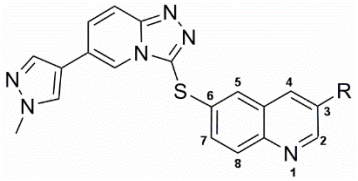		$T_{1/2}$ (min)				Volume (A^3)	ΔG (kcal/mol)	Docking score
Compound	R	Mouse	Rat	Monkey	Human			
63	-H	>500	>500	>500	>500	320.3	14.79	-18.4
68		307	431	271	>500	423.0	8.98	-15.5
2		>500	>500	>500	>500	409.0	14.68	2.0
23	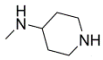	>500	>500	>500	>500	427.6	7.49	-15.6
5		>500	>500	>500	>500	409.5	8.44	-1.5
53	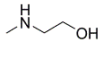	15	229	9.1	88	378.7	9.33	-21.9
15	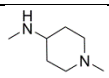	>500	287	414	>500	445.7	9.50	-9.4
47	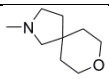	192	182	>500	464	466.8	10.90	-5.2
51		51	81	3.0	283	404.9	10.17	-22.6
11	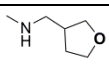	98	129	144	>500	423.0	10.71	-17.0
12		>500	>500	266	>500	412.6	10.99	-8.5

DMD Fast Forward. Published on September 12, 2018 as DOI: 10.1124/dmd.118.081919
This article has not been copyedited and formatted. The final version may differ from this version.

71		44	129	3.0	84	386.8	10.76	-20.4

DMD Fast Forward. Published on September 12, 2018 as DOI: 10.1124/dmd.118.081919
This article has not been copyedited and formatted. The final version may differ from this version.

Table 3. LC/MS/MS fragments of parent compounds (P) and their respective oxidative metabolites (M).

Parent compound (P)	Proposed metabolite (M) structure	$[M+H]^+$	Mass fragments
63	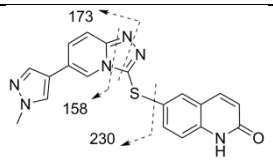	P: 359 M: 375	P: 146, 158, 173, 230 M: 146, 158, 173, 176, 230
53	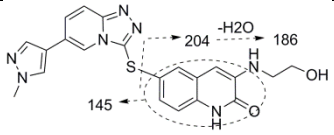	P: 418 M: 434	P: 146, 157, 173, 230, 375, 400 M: 145, 186, 204, 232, 416
51	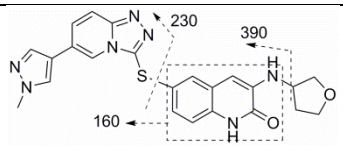	P: 444 M: 460	P: 158, 173, 230, 374, 416, M: 160, 230, 390, 442
11	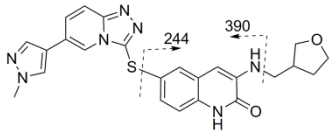	P: 458 M: 474	P: 173, 228, 259, 374, 386, 440 M: 173, 196, 227, 244, 390, 427, 456
71	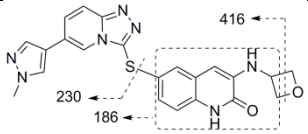	P: 430 M: 446	P: 158, 173, 230, 400 M: 145, 158, 186, 230, 416

DMD Fast Forward. Published on September 12, 2018 as DOI: 10.1124/dmd.118.081919
This article has not been copyedited and formatted. The final version may differ from this version.

Table 4. Inhibition of quinoline analogues metabolism by various molybdenum hydroxylase inhibitors in liver cytosol fractions.

		Percentage of control activity (%)					
	Species	Human	Human	Human	Human	Human	Mouse
Inhibitor (con.)	Analogue	**63**	**53**	**51**	**11**	**71**	**11**
Menadione(50μM)		20	9	22	49	9	7
Raloxifene (20μM)		23	2	13	65	2	14
Allopurinol (50μM)		118	83	92	110	86	98

DMD Fast Forward. Published on September 12, 2018 as DOI: 10.1124/dmd.118.081919
This article has not been copyedited and formatted. The final version may differ from this version.

Table 5. Kinetic study of quinoline analogues in liver cytosolic fractions from different species. Each triazolopyridine analogue (0.23-60 μM) was incubated with liver cytosolic fractions (0.1-1 mg/ml) for 30 min.

Species	Test compounds	V_{max} (pmol/mg/min)	K_m (μM)	V_{max}/K_m (μL/min/mg)
Mouse	**63**	14	38	0.36
	53	164	2.4	69
	51	25	1.0	25
	11	22	2.4	9.2
	71	28	1.7	16
Rat	**63**	1.8	64	0.03
	53	22	5.5	4.0
	51	19	1.1	17
	11	33	4.0	8.1
	71	11	1.0	11
Rabbit	**63**	7.1	64	0.11
	53	72	2.7	27

Monkey	**51**	95	4.3	22
	11	39	20	2.0
	71	229	5.9	39
	63	18	84	0.22
	53	23	2.6	8.8
Human	**51**	5.0	8.6	0.58
	11	14	63	0.23
	71	74	22	3.4

Fig.1

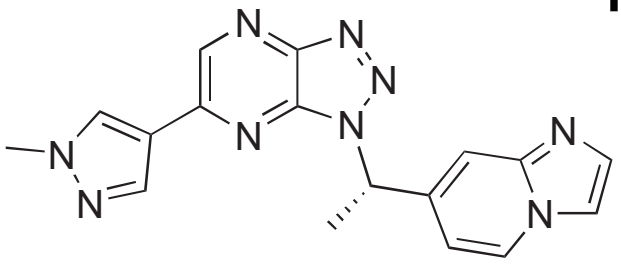

Savolitinib

Phase III

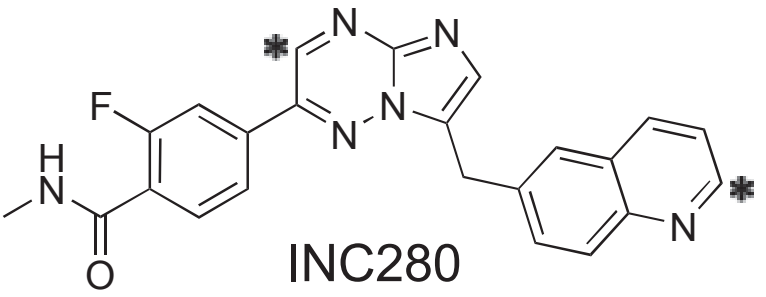

INC280

Capmatinib

Phase III

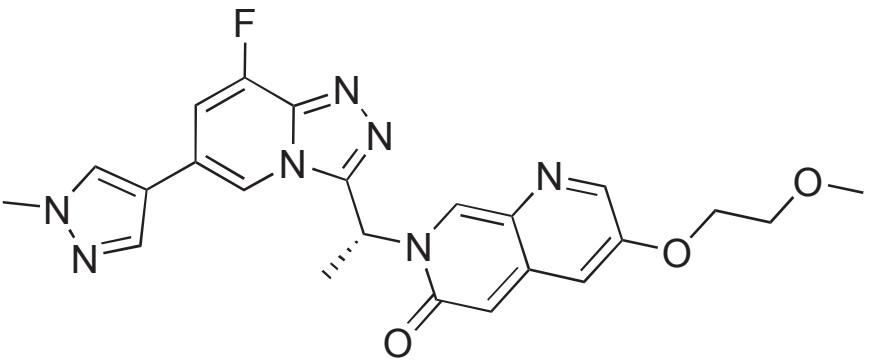

AMG-337

Phase II

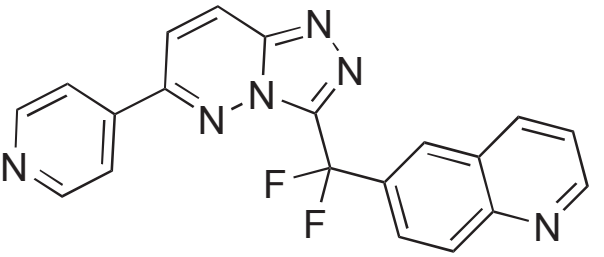

OMO-1

Phase II

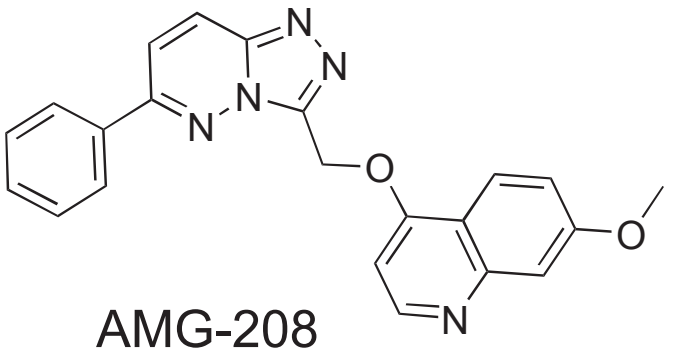

AMG-208

Phase I discontinued

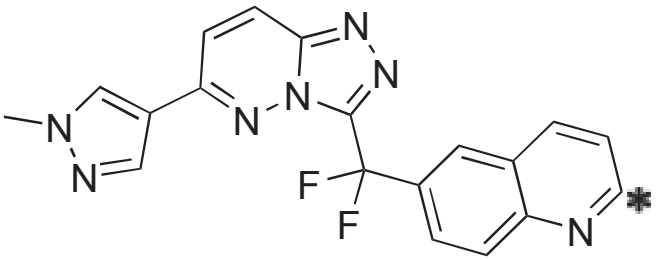

JNJ-38877605

Phase I terminated

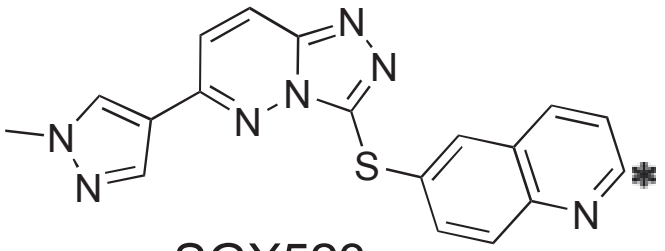

SGX523

Phase I terminated

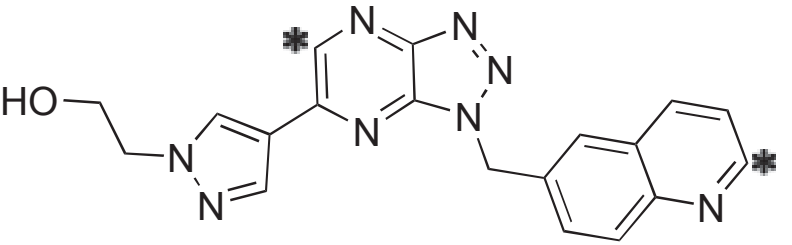

PF-04217903

Phase I terminated

Fig.2

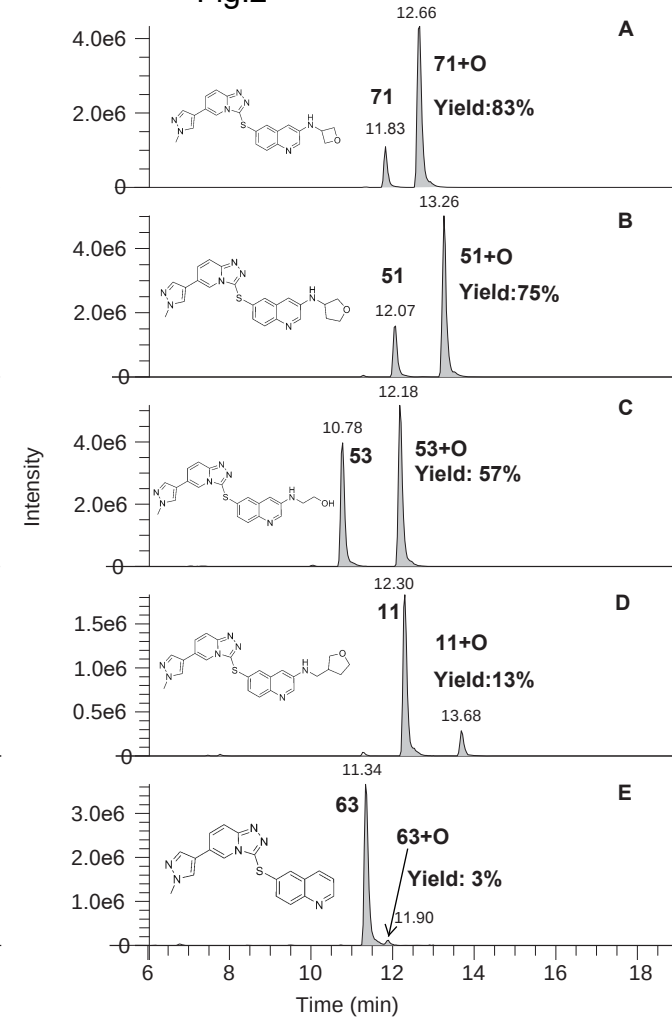
A
12.66
71+O
71
Yield:83%
11.83
4.0e6
2.0e6
0
B
13.26
51+O
51
Yield:75%
12.07
C
12.18
10.78
53
53+O
Yield: 57%
Intensity
D
12.30
11
11+O
Yield:13%
13.68
1.5e6
1.0e6
0.5e6
E
11.34
63
63+O
Yield: 3%
11.90
3.0e6
6
8
10
12
14
16
18
Time (min)

Fig.3

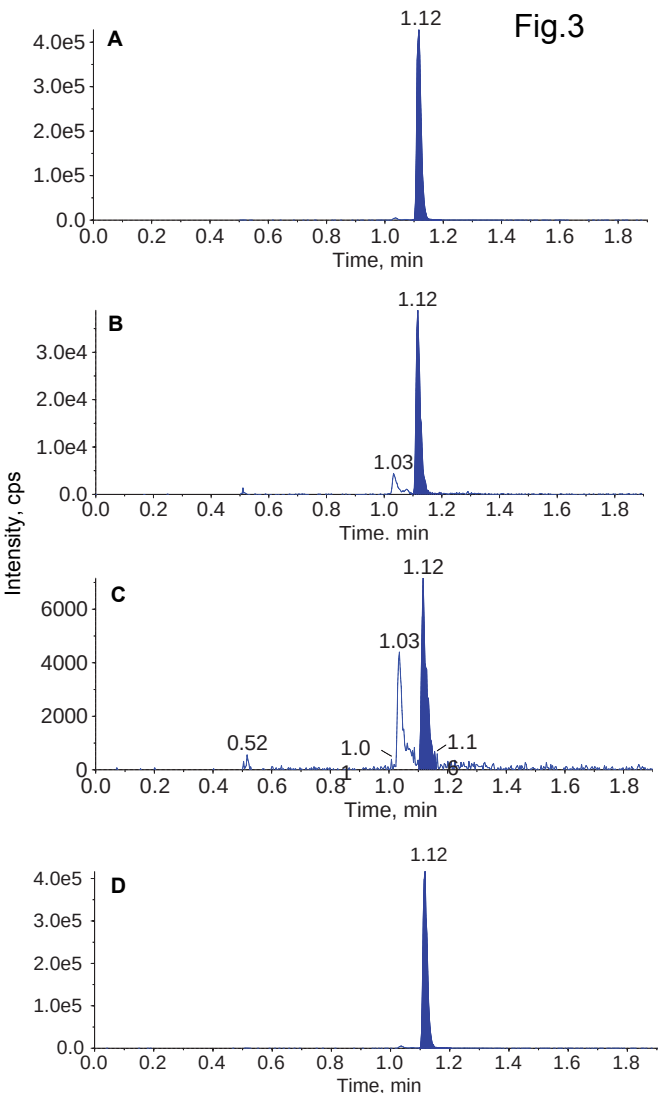
A
1.12
4.0e5
3.0e5
2.0e5
1.0e5
0.0
0.0 0.2 0.4 0.6 0.8 1.0 1.2 1.4 1.6 1.8
Time, min
B
1.12
1.03
3.0e4
2.0e4
1.0e4
0.0
0.0 0.2 0.4 0.6 0.8 1.0 1.2 1.4 1.6 1.8
Time. min
Intensity, cps
C
1.12
1.03
6000
4000
2000
0
0.52
1.0
1.1
0.0 0.2 0.4 0.6 0.8 1.0 1.2 1.4 1.6 1.8
Time, min
D
1.12
4.0e5
3.0e5
2.0e5
1.0e5
0.0
0.0 0.2 0.4 0.6 0.8 1.0 1.2 1.4 1.6 1.8
Time, min

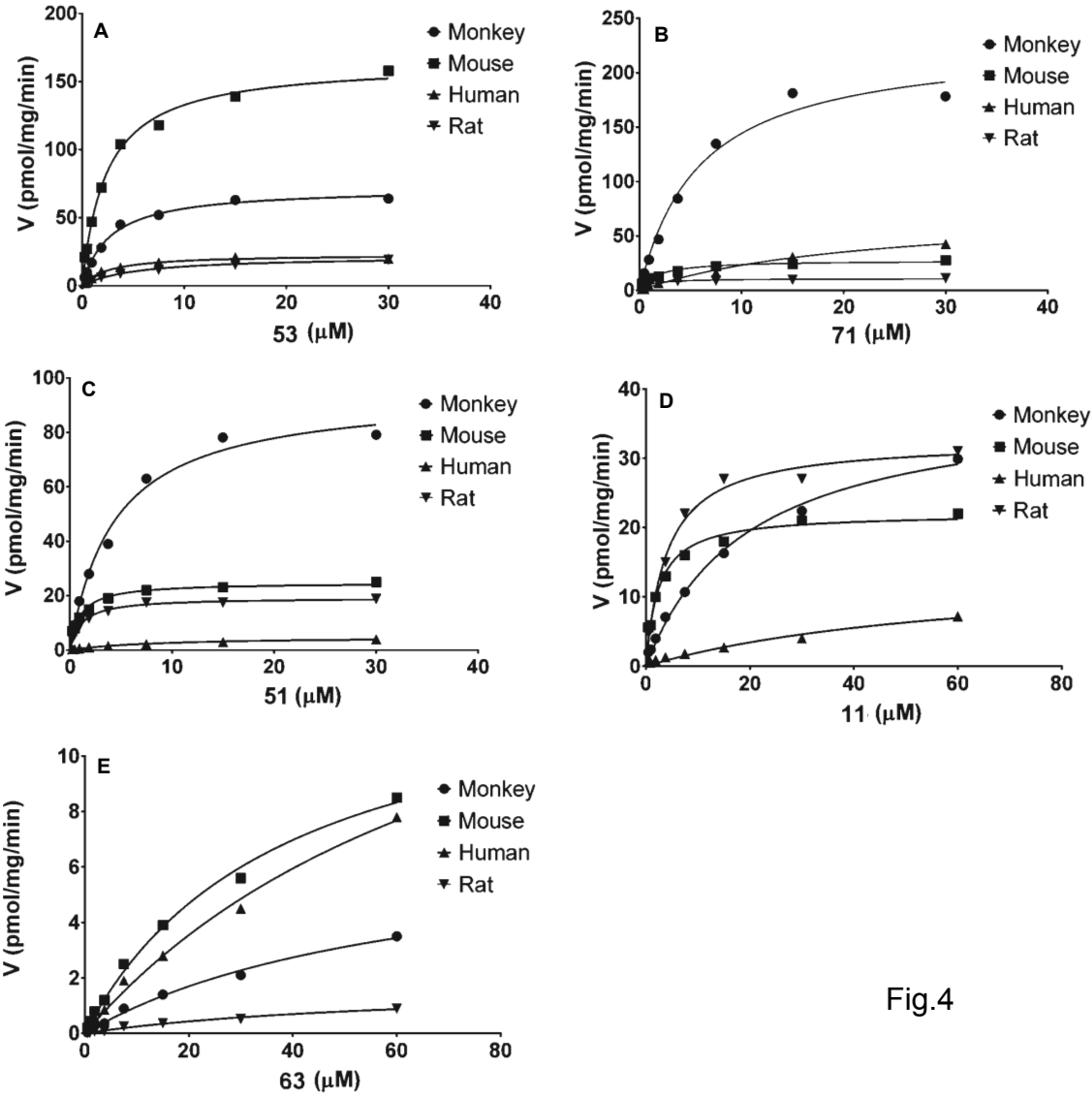
A
V (pmol/mg/min)
53 (μM)
Monkey
Mouse
Human
Rat
B
V (pmol/mg/min)
71 (μM)
Monkey
Mouse
Human
Rat
C
V (pmol/mg/min)
51 (μM)
Monkey
Mouse
Human
Rat
D
V (pmol/mg/min)
11 (μM)
Monkey
Mouse
Human
Rat
E
V (pmol/mg/min)
63 (μM)
Monkey
Mouse
Human
Rat

Fig.4

Fig.5

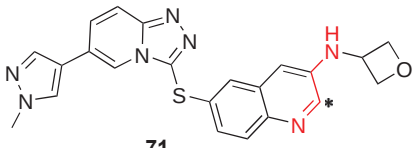

71

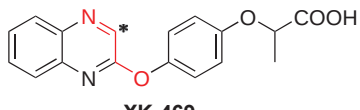

XK-469

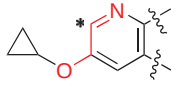

Unpublished example 1

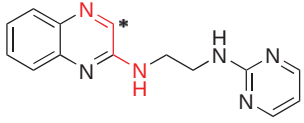

Example 2
Cruciani et al., 2018

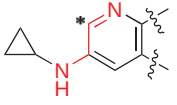

Unpublished example 2

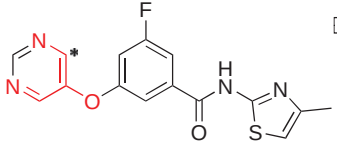

VU0409106

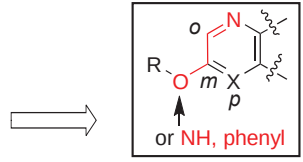

Proposed structure feature
with high AO liability
1) aza heterocycle
2) *o*-vacant C-H
3) *m*-smal EDG (O, N, phenyl, etc)

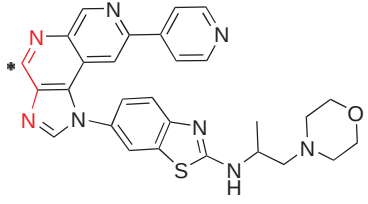

Example 30
Glatthar et al., 2016

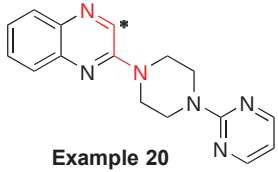

Example 20
Cruciani et al., 2018